JCTC Journal of Chemical Theory and Computation

ARTICLE

pubs.acs.org/JCTC

Modeling Molecular Crystals by QM/MM: Self-Consistent Electrostatic Embedding for Geometry Optimizations and Molecular Property Calculations in the Solid

Ragnar Bjornsson and Michael Bühl*

School of Chemistry, North Haugh, University of St. Andrews, St. Andrews, Fife, UK KY16 9ST, United Kingdom

Supporting Information

ABSTRACT: We present an approach to model molecular crystals using an adaptive quantum mechanics/molecular mechanics (QM/MM) based protocol. The molecule of interest (or a larger cluster thereof) is described at an appropriate QM level and is embedded in a large array of MM atoms built up from crystal structure information. The nonbonded MM force field consists of atom-centered point charges and Lennard-Jones potentials using van der Waals parameters from the UFF force field. The point charges are initially derived from a single molecule DFT calculation and are then updated self-consistently in the field of point charges. Additional charges are fitted around the MM cluster to correct for missing long-range electrostatic effects. The geometry of the central complex can then be relaxed by quantum chemical calculations in the surrounding MM reaction field, hence capturing solid-state effects on the geometry. We demonstrate the accuracy of this approach for geometry optimization by successful modeling of the huge gas-to-solid bond contraction of HCN-BF_3, the ability to reproduce periodic-DFT quality local geometries of solid $VOCl_3$, and the geometry of $[Ru(\eta^5\text{-}Cp^*)(\eta^3\text{-}CH_2CHCHC_6H_5)(NCCH_3)_2]^{2+}$, a difficult ruthenium allyl complex in the solid state. We further show that this protocol is well suited for subsequent molecular property calculations in the solid state (where accurate relaxed geometries are often required) as exemplified by transition metal NMR and EFG calculations of $VOCl_3$ and a vanadium catechol complex in the solid state.

1. INTRODUCTION

The gas phase is the natural reference state for molecular quantum chemistry. Modeling chemical systems in the condensed phase, be it solid or liquid, adds a whole new level of complexity on top of the electronic structure problem. Proper inclusion of the relevant environmental effects on molecular structures and properties is a major challenge for computational chemistry. Thus, the quest for reliable and affordable methods to achieve this goal continues unabated.

Periodic plane-wave density functional theory (DFT) calculations have become very popular for modeling the solid state where the translational crystal symmetry is used directly to make calculations of the infinite solid possible. Even the liquid state can be modeled by the periodic supercell approach. The periodic approach has its limitations, however, as one is often limited to GGA-DFT calculations (due to the heavy computational demand of the nonlocal Hartree−Fock exchange in hybrid functionals[1]), and approximations are usually made to the core electrons (making molecular property calculations troublesome). For crystals with very large unit cells, periodic calculations simply become too expensive.

Hybrid quantum mechanics/molecular mechanics (QM/MM) methods take a different approach to modeling environmental effects. The molecule or region of interest is described at an appropriate quantum mechanics level (QM), and the environment is described by classical potentials (molecular mechanics, MM). Electrostatic embedding, where the point charges of the MM region polarize the electron density of the QM region, typically accounts for the interaction between QM and MM regions as well as classical bonded and nonbonded short-range potentials. Special care is needed when the QM−MM boundary goes through a covalent bond, and various boundary schemes have been developed to account for this.[2,3]

The QM/MM approach has become very popular for treating large nonperiodic systems such as enzymes,[4] or for modeling solvent effects on reactions.[5,6] Because only a subset of atoms are treated quantum-mechanically, it is affordable to retain the real degrees of freedom of the full system and to account for specific long-range intereactions, albeit in a more approximative way. QM/MM approaches have also been used to model the solid state (sometimes called embedded cluster methods), such as the modeling of metal oxides, ionic crystals, surface catalysis, zeolite catalysis, polymers, etc.[7−11]

Advantages of QM/MM methods include the ability to move readily beyond GGA-DFT to hybrid-DFT methods for improved accuracy or even to more accurate wave-function-based methods for the QM region, all-electron calculations of core properties, and the possible inclusion of relativistic effects by one of the many all-electron approximations to the four-component Dirac equation. The disadvantages of QM/MM approaches are mainly the approximations that have to be made when dividing up the system: the need for an accurate MM force field, the approximate interaction term between QM and MM regions, and ionic or polymeric systems requiring special care for QM−MM boundaries.

Received: November 16, 2011
Published: December 16, 2011

A special type of solid-state system is molecular crystals. Small organic or inorganic compounds can crystallize due to attractive intermolecular interactions, and hence it is often the solid state where the structure determination of the compound takes place, for example, by X-ray crystallography and solid-state NMR, Mössbauer, EPR, IR, and Raman spectroscopies. While it is usually the single molecule properties that are of interest to the chemist, the solid state introduces crystal-packing effects due to the many intermolecular interactions between molecules in a crystal, and a polar crystal environment will inevitably influence molecular properties such as chemical shifts in NMR spectroscopy. Additionally, counterions and even crystallized solvent may significantly alter the picture of the environment surrounding each molecule, compared to a single molecule in the gas phase.

Molecular property calculations of molecules are often performed in the gas phase,[12] and a common theme in many such studies in the literature is the question of whether quantum mechanics optimized structures or X-ray structures should be used.[13−17] The X-ray structure represents a thermally averaged crystal-packed structure, but it is taken out of its solid environment and may not always be accurate. In particular, static or dynamic disorder, if gone undetected, can impart notable artifacts on individual geometric parameters, which are potentially detrimental to subsequent molecular property evaluations. Quantum mechanical optimizations in the gas phase, on the other hand, afford equilibrium structures lacking effects from thermal motion or the environment.

Two QM/MM-based approaches, called the embedded ion method (EIM)[18] and extended embedded ion method (EEIM),[19] have recently been successfully used to calculate NMR properties of molecular crystals and ionic solids[20] using self-consistent point charges and Ewald lattice sums, and a similar approach was used in a recent paper by us.[21] A QM/MM approach has also recently been used to model environmental effects on charge density distributions in the methyl lithium crystal.[22] These embedded molecular property calculations use either experimental X-ray geometries or in some cases optimized hydrogen positions,[20] while in ref 21 periodic-DFT optimized structures were used. Typically, QM/MM studies require a full-fledged force field (i.e., well-parametrized bonded and nonbonded terms of the whole molecule) for the MM region in order to perform geometry optimizations. This is not a problem when modeling proteins, for instance, for which many bespoke, well-parametrized force fields exist. On the other hand, for many inorganic or organometallic molecules, and especially transition metal complexes, force field parameters often are unavailable or of limited transferability.

Recent examples of molecular crystal modeling with QM/MM approaches include, e.g., the self-consistent Madelung potential semiempirical method (SCMP-NDDO),[23] the extended point charge and supermolecule (PCX and SMX) methods,[24] the hybrid QM/MM many-body interaction model,[25] modeling of proton transfer and polarons in crystalline diamino-dinitroethylene,[26] modeling of photocrystallographic properties of organic molecules in a crystal,[27] and QM/MM molecular dynamics simulations of organic (opto)electronic materials.[28]

In this paper, we present a QM/MM-based method to model solid-state effects on small molecules in a molecular crystal that does not require a full force field yet allows geometry optimization in the solid state. The method requires a starting crystal structure (e.g., from X-ray crystallography) but no system-specific parameters (except for van der Waals parameters, which here are general), is almost black-box, and can be easily automated. We demonstrate the accuracy of the method for geometry optimization using various examples and highlight the method's usefulness for molecular property calculations in the solid state, such as for anisotropic transition metal chemical shifts and quadrupole couplings.

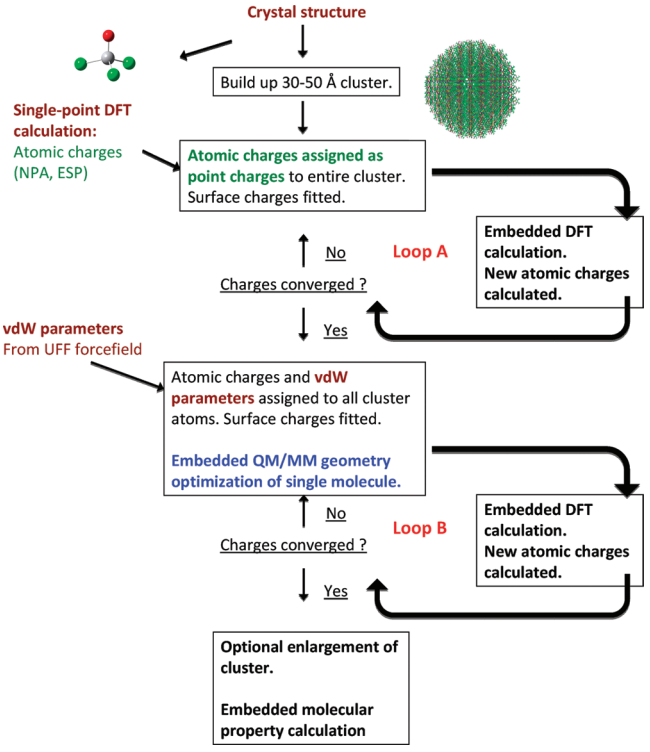

Figure 1. The self-consistent electrostatic embedding protocol for geometry optimization and molecular property calculations.

2. COMPUTATIONAL PROTOCOL

Our motivation comes from our desire for accurate molecular property calculations in the solid phase, such as first principles NMR calculations of solid-state NMR parameters[29] (which often include calculations of both chemical shift and electric-field gradient (EFG) tensors). Chemical shift calculations in particular tend to be sensitive to geometrical effects.[30] While experimental X-ray structures are often available, quantum chemical geometry optimizations are usually preferable, especially for hydrogen positions, as found by recent periodic DFT studies.[31−34] As periodic geometry optimizations can become very expensive as the unit cell gets larger, an attractive alternative would be to only relax the geometry of a single molecule within the solid phase. Our proposed QM/MM protocol allows one to do this.

The protocol is shown schematically in Figure 1 and is described as follows:

1. Crystal structure information from experimentation or another source is used to build up a large nonquantum cluster (typically with a radius of 30−50 Å) centered on one molecule. Atomic charges from a single molecule DFT calculation (at initial geometry) are then assigned to all other equivalent molecules in the cluster. If the cluster consists of multiple molecules, e.g., solvent or counterions, then charges for those need to be assigned as well.

2. Loop A: Additional surface charges are fitted on the outside of the cluster to emulate the electrostatic potential of the infinite periodic system. A single molecule DFT calculation of the central molecule, now embedded in the surrounding point charges, is carried out. The resulting atomic charges from a population analysis of that calculation are then assigned to all of the other equivalent classical molecules. The charge calculations, assigning, and surface-charge-fitting are updated self-consistently, typically until the charges change less than 0.0001*e*.
3. van der Waals parameters (vdW), taken from the UFF force field,[35] are assigned to all cluster atoms (including the QM atoms) and used to derive 6-12 Lennard-Jones (L-J) potentials for all atom pairs.
4. Loop B: A QM/MM geometry optimization is performed, keeping only the QM region (the central molecule) active. All classical atoms (each having only an assigned charge and vdW parameter) are kept frozen and interact only statically with the QM region using the previously derived point charges and L-J potentials. When the QM geometry converges, new atomic charges are calculated, which are subsequently assigned to all other cluster atoms. Geometry optimization and charge iterations on the new updated cluster are performed until the charges are self-consistent and/or no further optimization steps are required.
5. If resources allow, the QM region can be enlarged at this stage to include nearest neighbors to the central molecule. A geometry optimization is then performed using the previously determined point charges and with either the nearest neighboring units fixed or active.
6. Finally, an embedded molecular property calculation can be performed, possibly with a larger QM region, on the QM/MM optimized geometry.

The above protocol is straightforward and can easily be automated when the molecular crystal is homogeneous (only one type of molecule) but requires slightly more user input when the crystal includes, e.g., solvent molecules, counterions, etc. The protocol allows freedom in choosing the quantum chemical method for geometry optimization, atomic charge calculation, and molecular property calculation (may be different). The protocol would even allow for a molecular dynamics treatment of the QM nuclei. The QM method may be a specific DFT functional or even a wave-function-based method and basis set, possibly including a relativistic treatment of electrons. The choice will obviously be a balance between computational cost and required accuracy.

How the atomic charges are calculated also allows some flexibility, as they can be defined in many different ways. In this work, we have performed trials of ESP charges (i.e., charges that reproduce the electrostatic potential),[36] NPA charges (from Natural Population Analysis),[37] and Mulliken charges.[38] The ESP charges (without restraints) were calculated with a procedure in Chemshell[39] (here denoted ESP), according to the protocol described in ref 36. The vdW radii used for both vanadium and ruthenium atoms in the ESP calculations were 3.0 Å and were in addition scaled by 1.5. Trials of ESP charges according to the Merz−Kollman protocol[40] as implemented in Gaussian 09 (denoted ESP-MK) were also performed using a vdW radius of 2.0 for vanadium.

The vdW parameters have all been taken from the UFF force field, which is available for almost the whole periodic table. The suitability of these parameters for the current purpose is unknown. If one wishes, available system-specific parameters, Lennard-Jones parameters, can be chosen instead as can other types of short-range potentials. For simplicity, 6−12 L-J potentials with UFF parameters are always used here. We note that other intermolecular interactions such as charge-transfer are not explicitly modeled by our approach, and the exchange-repulsion and dispersion are only modeled classically. Since there is here no quantum mechanical expression for the exchange-repulsion between QM and MM atoms, charge leakage may possibly occur where electron density may "leak" out to the positive point charges, an artifact that would be prevented by exchange-repulsion in a full QM system. This effect is closely related to overpolarization effects. It has been shown, however, that charge leakage tends not to be a problem in QM/MM calculations as long as no overly diffuse basis sets are used.[41] This problem tends to come to the fore when covalent bonds are cut and saturated with link atoms, which is not necessary in our cases.

We note that the effective fragment potential method[42] presents a more elaborate approach to deriving the MM parameters from ab initio calculations and includes a multipole expression for the Coulomb interactions and expressions for induction, exchange-repulsion, dispersion, and charge-transfer, all parameters derived from ab initio calculations. In our approach, the lack of some of these interactions in the energy expression can be alleviated by increasing the QM region to better account for the short-range interactions but which obviously can become expensive, even for small molecules, as many nearest neighboring molecules might need to be included. Smaller basis sets, possibly with effective core potentials, can, however, be used to make such calculations tractable. Another possibility might be to combine the frozen-density embedding method[43] with our protocol. Point-charge smearing around the QM region to prevent overpolarization by the point charges could also be explored.[44]

The main advantages of our QM/MM approach are that it is in principle applicable to every kind of molecular crystal (as long as one is interested in local properties), is not dependent on the availability of force field parameters for each type of molecule, and has low computational cost and simplicity. Since only the QM region is being optimized, only external vdW parameters need to be supplied, while the point charges are computed from theory. The decision to only optimize the QM region (i.e., keep the entire MM region frozen) is due to the lack of MM parameters for the full system. Only nonbonded MM terms are supplied, and hence MM coordinates cannot be free variables. It is possible, however, to allow the MM region to be active if one freezes all internal coordinates of the MM molecules. This remains to be explored.

Solid $VOCl_3$ was optimized using the CPMD program[45] in a periodic supercell with dimensions $10.046 \times 9.216 \times 11.278$ Å^3 containing a total of eight independent molecules, which corresponds to the experimental structure of Troyanov,[46] doubled along the *a* axes in order to avoid *k*-point sampling. Norm-conserving Troullier−Martins pseudopotentials were used in the Kleinman−Bylander form, and Kohn−Sham MOs were expanded at the Γ-point in a basis of plane waves with a cutoff of 320 Ry to minimize basis set effects on the geometries.[47] The solid structure of the vanadium catechol complex **4** was optimized in the trigonal crystallographic unit-cell with a fixed size of $6.77 \times 10.72 \times 12.15$ Å^3 with $\alpha = 98.40°$, $\beta = 92.13°$, and $\chi = 94.05°$. The same set of pseudopotentials as for $VOCl_3$ was used,

Chart 1

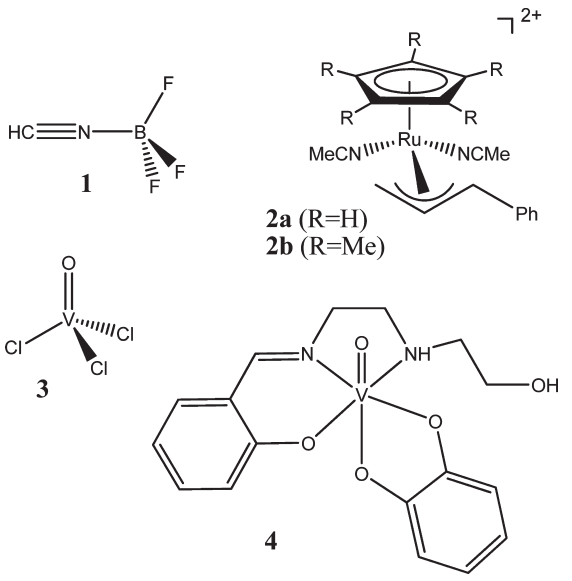

and MOs were expanded at the Γ-point in a basis of plane waves with a cutoff of 200 Ry.[48]

All QM/MM calculations have been performed using Chemshell,[9,39] a general purpose QM/MM program which links together different QM programs and MM programs. The built-in MM program DL_POLY[49] was used in this work for handling the force field parameters, while Turbomole version 6.0[50] and Gaussian 09[51] were used for QM calculations (other programs such as NWChem,[52] ORCA,[53] GAMESS-UK,[54,55] Molpro,[56] MNDO,[57] and others can also easily be linked with Chemshell). DL-FIND[58] as implemented in Chemshell was used for all geometry optimizations. The cluster build-up and fitting routines are part of Chemshell and were written by Thomas Keal based on algorithms originally developed by Alexey Sokol. NMR and EFG calculations have employed the Gaussian 09 program (^{51}V chemical shifts of **4** are given relative to gaseous $VOCl_3$, **3**, optimized at the same level of theory).

By giving crystal structure information as input and specifying the size of the cluster, QM method, charge model, and vdW parameters, steps 1−4 of our protocol can be performed automatically in a single Chemshell input file, as long as the crystal is homogeneous. More complex crystals require slightly more user input. Scripts to carry out the protocol will be made available in a future version of Chemshell. The specific setup, notably the exchange-correlation functional and basis set, are detailed in the corresponding Results subsections. The target systems of this study are sketched in Chart 1.

3. RESULTS FOR SELECTED TEST SYSTEMS

3.1. Modeling the Gas-to-Solid Bond Contraction in HCN-BF_3. Molecules can have distinctly different geometries in the gas phase and the solid phase. The Lewis acid−base complex HCN-BF_3 (**1**) is a good example of such behavior. According to a microwave study,[59] the B−N bond length is 2.473 Å in the gas phase, while the X-ray solid-state structure[60] shows a B−N bond length of 1.638 Å, corresponding to a gas-to-solid bond contraction of 0.835 Å. Similar to the related BH_3−NH_3,[61] this large bond contraction has been attributed to both the crystal dipolar

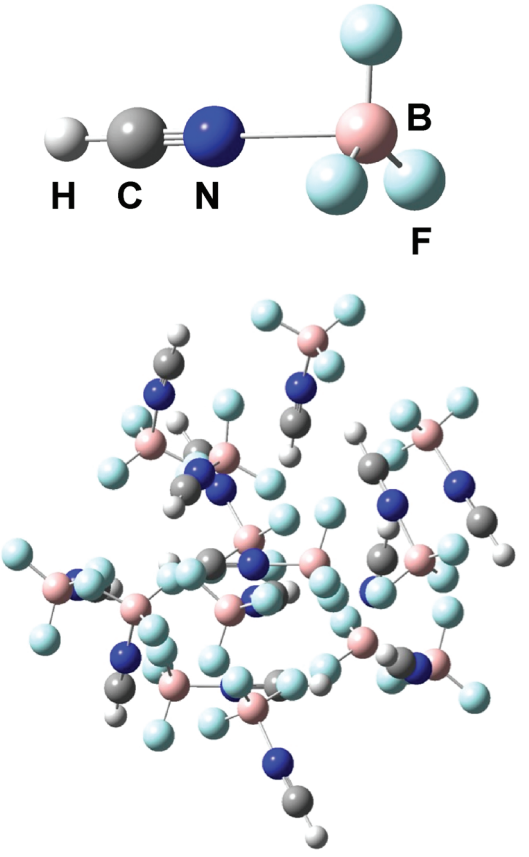

Figure 2. Cluster 1 (top) and cluster 2 (bottom) models used in QM/MM calculations of solid HCN-BF_3 (**1**).

field interaction in the solid[62] as well as nearest neighbor short-range interactions.[63]

The gas phase structure of HCN-BF_3 and other related compounds presents a challenge to theory on its own. Phillips and Cramer[64] and others[65] have studied HCN-BF_3 and other related molecules and found that these molecules present difficulties for many DFT approximations and wave function methods. GGA and meta-GGA functionals often perform very poorly, and hybrid functionals like B3LYP[66,67] still give bond length deviations of 0.06 Å. The hybrid functional B3PW91[66,68] was found to give a satisfactory equilibrium geometry for HCN-BF_3 with a B−N bond length of 2.465 Å, despite not giving a satisfactory binding energy.[64] Equilibrium geometries were also found to be close to vibrationally averaged geometries.[64]

We applied our QM/MM approach to this system in order to see how well such a demanding system can be modeled, especially the gas-to-solid B−N bond contraction. As the molecule is small, this further allows one to expand the cluster to include nearest neighbors (step 5 of our protocol). As the B3PW91 functional is able to reproduce the gas phase structure quite well (in contrast to other DFT methods), we chose it for geometry optimization and atomic charge calculations. We note that it is unclear why this functional should perform so much better than other functionals and is probably due to error cancellations to some extent. A wave function method capable of accurately describing medium- to long-range electron correlation effects seems to be necessary for a satisfactory description of this difficult system.[64] We note that it is perfectly possible to use higher level methods in our protocol such as double hybrid functionals[69] or

Table 1. Geometric Parameters of HCN-BF_3 from B3PW91/aug-cc-pVTZ Calculations in the Gas Phase and in the QM/MM Solid[a]

		QM/MM Mulliken	QM/MM NPA			QM/MM ESP-MK				
	gas	cluster1	cluster1	cluster2 frozen	cluster2 relaxed	cluster1	cluster2 frozen	cluster2 relaxed	exptl. gas[b]	exptl. solid[c]
B−N bond length (Å)	2.465	1.572	1.610	1.618	1.614	1.625	1.616	1.609	2.473	1.639
gas−solid diff. (Å)		0.893	0.855	0.847	0.851	0.840	0.849	0.856		0.834
N−B−F angle (deg)	93.5	107.9	105.9	106.0	106.2	105.4	106.1	106.3	91.5	105.6
gas−solid diff. (deg)		−14.4	−12.4	−12.5	−12.7	−11.9	−12.6	−12.8		−14.1
C−N−B angle (deg)	180.0	175.3	175.2	177.8	177.4	175.3	177.8	177.2	180.0	178.5
C−N bond length (Å)	1.143	1.135	1.134	1.135	1.135	1.133	1.135	1.135	n.a.	1.121

[a] See Figure 2 for definition of clusters 1 and 2. [b] From ref 59. [c] From ref 60.

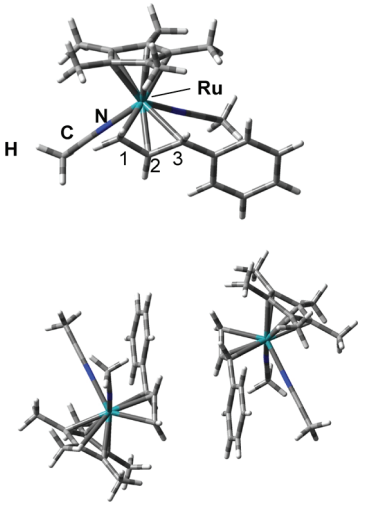

Figure 3. The monomeric (top) and dimeric structures (bottom) of the ruthenium allyl complex **2b**.

even coupled cluster theory, but that is outside the focus of our study. We have thus for now just used the B3PW91 functional for all gas and solid calculations.

Using the experimental X-ray structure,[60] a cluster with a radius of 37 Å was built. Mulliken, NPA, and ESP-MK charges for electrostatic embedding were compared. B3PW91 and the aug-cc-pVTZ basis set[70] were used for charge calculations and geometry optimization, and the QM program was Gaussian 09.

The self-consistent loop A (see Figure 1) was iterated six times, until the charges changed less than 0.0001*e*. Loop B was iterated four times until the gradient stopped changing between charge iterations.

The QM cluster was then increased to include the 13 nearest neighboring molecules, as shown in Figure 2. The aug-cc-pVTZ basis set was used for the central molecule but the smaller 6-31G* basis set[71] for the neighbors. Two different geometry optimizations were carried out (both using the previously determined self-consistent charges): one with the nearest neighbors frozen at experimental coordinates and the other optimization allowing all molecules to move. These larger QM optimizations were only performed using NPA and ESP charges.

Selected bond lengths and bond angles for the central molecule from the different geometry optimizations are shown in Table 1. The B3PW91/aug-cc-pVTZ gas phase structure shows acceptable agreement compared to the experimental gas phase structure as deduced from the B−N bond length and N−B−F angle. The solid-state QM/MM optimizations using only a single molecule and with three different charge models for the environment reveal that the B−N bond contraction is very well reproduced using NPA and ESP charges but less so using Mulliken charges. This is not surprising, as Mulliken charges are known to be strongly basis set dependent and often rather unreliable.[72] Increasing the QM cluster from a single molecule to 14 molecules (neighbors frozen) results in rather small differences for both NPA and ESP charge model systems, suggesting that the QM−MM interaction term (electrostatic embedding + L-J potentials) is capable of describing most of the necessary intermolecular effects that influence the potential energy surface of **1**. The C−N−B angle, which deviates slightly from linearity in the single molecule QM/MM optimizations, is improved when including nearest neighbors. Allowing all 14 molecules to move only results in small changes in bond lengths and angles of the central molecule.

These results are encouraging, as they suggest that accurate molecular structures can be obtained in a molecular solid using only electrostatic embedding and classical short-range potentials, even for a molecule that experiences huge geometric differences between the gas and solid.

3.2. Solid-State Effects on the Weak Ru−C Interaction in an Ru(IV) Allyl Complex. In a recent study by Calhorda et al.,[73] the geometry of the Ru(IV) allyl dicationic complex, $[Ru(\eta^5\text{-}Cp)(\eta^3\text{-}CH_2CHCHC_6H_5)(NCCH_3)_2]^{2+}$ (**2a**), was calculated at several DFT levels and compared to the experimental X-ray structure[74] of the analogous $[Ru(\eta^5\text{-}Cp^*)(\eta^3\text{-}CH_2CHCHC_6H_5)(NCCH_3)_2]^{2+}$ (**2b**, Cp* instead of Cp). It was found that all levels of theory gave an unsatisfactory description of the coordination mode of the η^3-allyl unit as evidenced by the 0.2−0.5 Å deviation from the experimental value for the Ru−C3 bond (C3 being the substituted allyl carbon). As DFT calculations on 4d transition metal complexes typically give bond length deviations of 0.02−0.03 Å according to recent benchmark studies,[75] these large deviations were interpreted as a failure of current DFT approximations to describe the Ru allyl binding. PBE0[76] in particular has been found to give very good geometries for 4d and 5d transition metal complexes; hence, its failure to describe the Ru-allyl coordination mode is surprising.

Truhlar and Kulkarni[77] found that simplifying the experimental complex **2b** to **2a** in the gas phase is not entirely appropriate, and newer density functionals like M06-L,[78] M06,[79] SOGGA,[80] and ωB97X(-D)[81] were found to give Ru−C distances in better agreement with experimental results when calculating the real

Table 2. Geometric Parameters of the Ru−Allyl Complex, 2b, from PBE0(-D) Calculations on Monomeric and Dimeric Units in the Gas Phase and in the Solid[a,b]

		gas		QM/MM ESP	QM/MM NPA	QM/MM ESP	QM/MM NPA
		monomer				dimer	
	exptl.[c]	PBE0	PBE0-D	PBE0-D	PBE0-D	PBE0-D	PBE0-D
Ru−C1	2.181	2.156 (0.025)	2.157 (0.024)	2.157 (0.024)	2.165 (0.016)	2.161 (0.020)	2.160 (0.021)
Ru−C2	2.189	2.202 (−0.013)	2.185 (0.004)	2.167 (0.022)	2.170 (0.019)	2.170 (0.019)	2.168 (0.021)
Ru−C3	2.382	2.501 (−0.119)	2.426 (−0.044)	2.360 (0.022)	2.346 (0.036)	2.354 (0.028)	2.351 (0.031)
Ru−CR	2.222	2.219 (0.003)	2.209 (0.013)	2.206 (0.016)	2.207 (0.015	2.206 (0.016)	2.207 (0.015)

[a] Bond lengths and deviations (exptl. − calcd., in parentheses) in Å. [b] See Figure 3 for monomer and dimer structures. [c] From ref 74.

system **2b**. Nevertheless, the Ru−C3 distance was still an outlier for all functionals. Jacobsen[82] recently reassessed the problem and made a case for crystal packing effects being responsible for the deviation from experimental results as argued from semiempirical lattice energy calculations.

As our QM/MM method should be able to account for some of the intermolecular forces responsible for such proposed crystal packing effects, we carried out calculations on **2b**. Using the experimental crystal structure[73] (PF_6^- counterions and cocrystallized acetone), a cluster with a radius of 42 Å was built. The initial QM region consisted of a single dicationic Ru complex which was later expanded into a dimer (see Figure 3). Charge iterations and geometry optimizations of the QM region were performed at the PBE0 level using the mixed def2-TZVPP/def2-SVP basis set[83] (metal/ligand, with the accompanying ECP on Ru) with and without the DFT-D dispersion correction by Grimme,[84] performing trials for both ESP and NPA charges. Only charges for the Ru complex were iterated, while charges for PF_6^- anions and acetone solvent molecules were kept fixed at gas phase values from DFT calculations at the same level of theory. Turbomole was used as a QM program for geometry optimizations, while the (embedded) charge calculations were performed with Gaussian 09.

The results obtained in the gas phase and in the QM/MM embedded cluster are shown in Table 2. Comparing gas phase PBE0 and PBE0-D results reveals that intramolecular dispersion has a substantial effect on the Ru−C3 bond by shortening it by 0.075 Å, and the deviation between theory and experiment is improved from 0.119 Å to 0.044 Å. However, the environment seems also to have an effect: when the dication is allowed to relax at the same DFT level but in the embedded crystal, there is a further shortening of 0.066 or 0.080 Å (depending on the use of ESP or NPA charges), resulting in even better agreement with experimental results for the Ru−C3 bond. The Ru−C3 equilibrium distance from the QM/MM calculations becomes shorter than the experimental value.[85] QM/MM geometry optimization of a dimer (using converged charges from the monomer calculation) was also performed, i.e., a pair of enantiomers, yielding additional shortening. Our results are thus in agreement with Jacobsen's argument that intermolecular effects in the solid state affect the Ru−allyl bonds, although intramolecular dispersion has an equally large effect, which would also explain the results from Truhlar et al., as the best performing functionals in that study were developed to account for dispersion effects. Ideally, both intramolecular and intermolecular effects should be reliably taken into account in any study of a molecule in the solid state (see, e.g., ref 86).

We emphasize that our results are not real predictions of how the molecule behaves in the solid, as experimental crystal structure information is directly used in our protocol (this is, however, usually the case in any kind of modeling of the solid state). One might argue that all we have done is to put experimental constraints on the system. Nevertheless, we have been able to demonstrate that when a simple account of environmental effects by electrostatic embedding and short-range potentials is made, there is no considerable disagreement with experimental and DFT results. And when the cluster is enlarged to a dimer, which introduces more quantum effects and relaxes some of the experimental constraints, very similar results are still obtained. We agree with Jacobsen that for a final unbiased reliable assessment of this system, full periodic DFT optimizations need to be performed at an appropriate DFT level where both the molecular geometry and lattice constants are allowed to relax. Nevertheless, our QM/MM method seems like a promising tool to capture solid-state effects on small molecules, for direct comparison with crystal-structure data where strong crystal-packing effects can be expected.

3.3. Solid-State ^{51}V NMR Parameters of $VOCl_3$: Comparison of Periodic and QM/MM Geometries. In a previous study, we had looked at anisotropic ^{51}V NMR parameters of $VOCl_3$ (**3**) in the solid state.[21] Periodic BP86-D[87,88,84] calculations based on the crystal structure from Troyanov[46] (with fixed experimental lattice parameters) were carried out with subsequent single-point embedded NMR calculations. We demonstrated the convergence of NMR parameters with increasing cluster size. An obvious drawback of the approach was the need for periodic DFT optimizations to get an accurate molecular structure from which to build the cluster model. While inexpensive for the small unit cell of $VOCl_3$, periodic DFT calculations will not always be affordable for larger crystals. We have now performed electrostatically embedded geometry optimizations in order to see how they compare to periodic DFT optimizations.

QM/MM geometry optimizations with the BP86-D functional and the large def2-QZVPP basis set[83] (same level for the charge calculations) were carried out on a 48 Å cluster built from the nonoptimized Troyanov structure, using three different charge models for point charge embedding: Mulliken, ESP, and NPA charges. Gas phase BP86-D/def2-QZVPP calculations were carried out as well.

Instead of comparing the geometric parameters directly, we assess the anisotropic NMR and EFG parameters themselves,[89] evaluated by single-point calculations on nonembedded single $VOCl_3$ molecules, taken from different geometry optimization protocols. The B3LYP functional was used for the NMR and

Table 3. Non-Embedded Anisotropic Chemical Shift and EFG Parameters[a] (B3LYP/QZVPPuncon/6-31G*) on $VOCl_3$ Geometries from Different Sources[b]

	periodic opt.	X-ray[c] Troyanov	X-ray[d] galy	gas opt.	QM/MM Mulliken	QM/MM ESP	QM/MM ESP-MK	QM/MM NPA
σ_{iso}	−2325.36	−2249.51	−2202.44	−2340.87	−2358.37	−2333.36	−2339.82	−2340.21
δ_σ	380.00	378.36	389.90	395.94	341.95	377.31	376.49	377.12
η_σ	0.016	0.018	0.004	0.000	0.047	0.023	0.021	0.014
C_Q	6.88	6.45	6.33	7.46	7.04	7.19	7.09	6.85
η_Q	0.078	0.036	0.037	0.001	0.016	0.039	0.058	0.120

[a] See ref 89 for definition of the NMR and EFG parameters. [b] Molecular geometry optimizations were performed at the BP86-D/def2-QZVPP level. [c] From ref 46. [d] From ref 90.

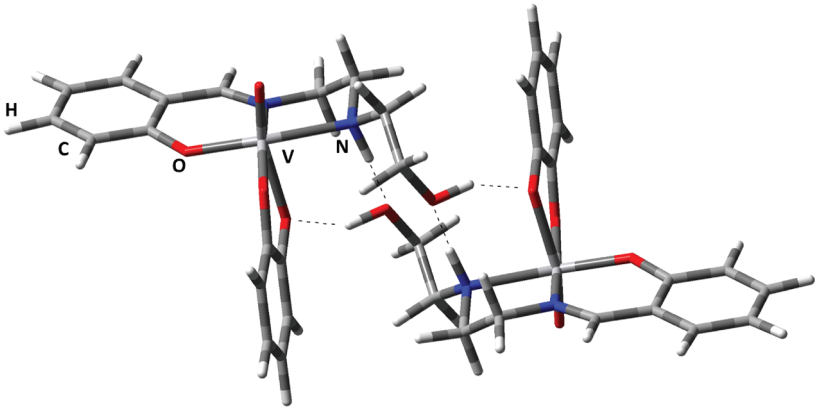

Figure 4. The dimeric structure of the vanadium catechol complex (**4**).

EFG calculations with the large uncontracted def2-QZVPP basis set on the vanadium atom and the 6-31G* basis set on O and Cl. Ideally, the QM/MM geometry optimizations would perfectly reproduce the results obtained using the periodic BP86-D geometry (assuming perfect basis set convergence in both cases and negligible errors from the pseudopotential in the periodic DFT calculation), and hence we can compare different QM/MM protocols.

Table 3 reveals that the NMR and EFG parameters obtained on the QM/MM optimized geometries with NPA or ESP charges are closer to the periodic results than the results from a gas phase calculation. The QM/MM Mulliken results are not as good. Results obtained on geometries from the Troyanov and a second X-ray structure[90] also reveal how sensitive the shielding can be to geometric effects from slightly different experimental setups.

On the basis of these results and the HCN-BF_3 results, it appears that in our QM/MM optimizations Mulliken charges are outperformed by NPA or ESP charges. While **3** does not show large solid-state effects on the geometry (as seen through the NMR parameters), these results are still encouraging and suggest that inexpensive QM/MM optimizations can furnish good approximations to fully periodic DFT geometries and are preferable to gas phase optimizations for NMR calculations.

3.4. The Disagreement between Computed and Observed ^{51}V Solid-State NMR Parameters of a Vanadium Catechol Complex. Chatterjee et al. recently published a solid-state NMR study on a series of "noninnocent" vanadium(V) catechol complexes.[16] One of the complexes was subjected to DFT calculations of the anisotropic shielding and EFG parameters,[89] which revealed considerable disagreement with experimental results. The results were also found to be sensitive to the geometry used and to the basis set used.

Suspecting a solid-state effect to be the main reason for the disagreement between theory and experimental results, we carried out QM/MM geometry optimizations on a 42 Å cluster, using the same X-ray structure[91] as in the work by Chatterjee et al. Inspection of the crystal revealed the presence of two enantiomers of the molecule and hydrogen bonds between the hydroxyl group of one enantiomer with one of the metal-binding oxygen atom of the other enantiomer as well as between the NH and hydroxyl groups (see Figure 4). As these hydrogen bonds may influence the charge density around the V atom and influence the V−O and V−N bond lengths (on which the NMR parameters may strongly depend), we performed calculations with either a monomer or a dimer in the QM region. The latter optimization was performed after relaxation of the monomer (using the monomer converged charges).

QM/MM geometry optimizations were performed at the BP86-D level using the def2-TZVPP basis set on V, N, and O atoms and def2-SVP on C and H. Charge calculations were performed at the same level. Single-point embedded NMR and EFG calculations were performed at the B3LYP level on both monomer and dimer structures. In order to minimize basis set effects in the NMR and EFG calculations, the large uncontracted def2-QZVPP basis set was used on the V atoms and the 6-31G* basis set on O, N, C, and H atoms, as has been found beneficial for EFGs.[92,93] A single $VOCl_3$ molecule, calculated at the same level of theory, was used as a reference for evaluating isotropic chemical shifts.

Additionally, periodic DFT optimizations were performed at the BP86-D level in order to see the influence of a periodic DFT optimized geometry on the NMR parameters. The optimized geometry was then subjected to the QM/MM-NPA protocol but without geometry optimizations, in order to get self-consistent

Table 4. Anisotropic NMR and EFG Parameters[a] of Vanadium Catechol Complex 4 (in Normal Face, Monomer; in Italics, Dimer[b])

geometries:		gas opt	X-ray		X-ray H-opt (gas)	QM/MM ESP		QM/MM NPA		periodic geo.	
parameter	exptl.[c]		nonemb.	emb.	nonemb.	nonemb.	emb.	nonemb.	emb.	nonemb.	emb.
δ_{iso}	58 ± 5	−53.4	54.4	−66.8		−14.2	−108.8	31.2	−139.0	25.0	−203.3
		−246.5	*−76.2*	*−150.3*	*−104.4*	*−169.2*	*−179.3*	*−148.1*	*−182.3*	*−160.1*	*−261.4*
δ_{σ}	−243 ± 30	−421.3	−450.3	−389.4		−459.7	−407.2	−527.3	−402.3	459.0	−340.2
		−427.8	*−418.5*	*−401.7*	*−405.5*	*−397.8*	*−358.6*	*−447.8*	*−351.9*	*−434.8*	*−398.2*
η_{σ}	0.93 ± 0.05	0.91	0.94	0.82		0.99	0.88	0.99	0.87	0.95	0.75
		0.61	*0.78*	*0.66*	*0.68*	*0.62*	*0.65*	*0.66*	*0.73*	*0.71*	*0.52*
C_Q	±4.0 ± 0.1	9.30	7.33	7.05		9.35	8.97	7.59	6.89	6.52	5.26
		7.25	*7.46*	*7.58*	*7.37*	*6.72*	*6.35*	*5.33*	*−4.62*	*6.00*	*5.58*
η_Q	1.00 ± 0.05	0.58	0.42	0.44		0.43	0.45	0.53	0.58	0.61	0.77
		0.64	*0.38*	*0.41*	*0.31*	*0.57*	*0.64*	*0.79*	*0.99*	*0.63*	*0.75*

[a] See ref 89 for definitions of the NMR and EFG parameters. [b] Evaluated at the B3LYP/QZVPPuncon/6-31G* level on BP86-D geometries (basis set: def2-TZVPP on V, O, and N; def2-SVP on C and H); see Figure 4 for the structure of the dimer. [c] From ref 16.

charges for the environment. Single-point NMR and EFG calculations on monomer and dimer structures were then performed, with and without point charges.

The monomer results in Table 4 (in normal face) reveal similar deviations from experimental results for the solid-state NMR parameters as in the DFT calculations from the Chatterjee et al. study.[16] Using a gas phase optimized geometry results in a too large C_Q value and a too low asymmetry parameter, η_Q, while the shielding parameters compare well to experimental results. We note that ^{51}V C_Q values from DFT calculations typically have errors of 1 MHz according to recent studies by us,[92,93] and the deviation between theory and experimental results on the order of 5 MHz seems thus uncomfortably large. Using an X-ray geometry results in a C_Q value closer to experimental results, but the asymmetry parameter gets worse. The calculated isotropic chemical shift is in very good agreement with experimental results, but including the embedded point charges in the NMR calculations results in worse agreement. QM/MM optimizations of the monomer were performed using both NPA and ESP charges. Curiously, there is a considerable difference in the results obtained, with the NPA results having a lower C_Q value. None of the monomer results give satisfactory agreement with experimental results for both shielding and EFG parameters, however.

When optimizing the dimer structure in the gas phase, only moderate improvement for the EFG value is obtained, and the shielding gets worse (see dimer results in italics in Table 4). Single-point energies on a dimer using the X-ray structure also do not show much improvement compared to monomer results, and optimizing the hydrogen positions (denoted H-opt in Table 4) also does not improve the numbers. However, when a dimer structure is QM/MM optimized using the previously determined self-consistent charges from the monomer calculations, the EFG parameters are in much better agreement with experimental results, especially when NPA charges are used rather than ESP charges. The 0.61 MHz deviation in the quadrupole coupling constant is comfortably close to the expected functional error of ∼1 MHz for ^{51}V quadrupole couplings and the asymmetry parameter is in excellent agreement with experimental results.[92,93]

When using the periodic DFT geometry instead of the QM/MM optimized geometry, the EFG tensor is also improved as compared to using the X-ray geometry (although of the opposite sign compared to the QM/MM−NPA optimizations). The results using QM/MM optimizations are closer to experimental results, however. It is not entirely clear why that is so. The QM/MM optimizations are all-electron calculations (as opposed to the periodic calculations that used pseudopotentials) and use a rather large basis set on the V, N, and O atoms, which should result in accurate metal−ligand bonds.

The shielding parameters from the QM/MM setup, δ_{iso} in particular, are not in very good agreement with experimental results. However, we attribute this to a failure of the DFT functional to describe strongly deshielded vanadium complexes as discussed in detail by Geethalakshmi et al.[94] In that study, an isotropic chemical shift of −5 ppm for the same compound was calculated in the gas phase at the B3LYP level with a different basis set and compared to the +220 ppm experimental chemical shift in solution. This deviation is significantly more than the typical ∼100 ppm deviation, which is typically found for ^{51}V chemical shifts.[95] Our gas phase B3LYP determined isotropic chemical shift is −53 ppm. The experimental shift in δ_{iso} in going from solution to the solid is −163 ppm. Our calculated gas to solid (QM/MM dimer with NPA charges) shift is −129 ppm (−208 ppm using the periodic geometry), hence suggesting that the environmental effect on the shielding tensor is at least partly being modeled correctly. It seems likely that the DFT functional error on the shielding tensor is dominating the errors in the absolute values from our calculations, preventing quantitative agreement with experimental results.

Our results show that accurate solid-state structures are crucial for accurate EFG parameters but also that specific hydrogen-bond interactions in the solid state may have to be included at the QM level for a correct description of these kinds of systems. Using NPA charges in our QM/MM protocol here results in much better agreement with experimental results than ESP charges. It is yet unclear why that is the case, but for now we are recommending the use of NPA charges in general. Overall, our QM/MM protocol presents itself as a much better starting point for solid-state NMR calculations of molecules than using either gas-phase optimized structures or X-ray structures.

In the single-point embedded NMR calculations, the density of the QM region is polarized by point charges of the MM region, but the classical L-J potentials obviously have no effect.

Charge leakage effects, as already discussed, could possibly occur here. Sebastiani and Rothlisberger[96] addressed this problem for NMR calculations by adding an exchange-repulsion expression directly into the QM region Hamiltonian of a plane-wave DFT code with some success. It is likely, however, that charge leakage is a much bigger problem with such intrinsically delocalized basis sets than with atom-centered basis sets as used in our work.

4. CONCLUSIONS AND OUTLOOK

We have presented a general QM/MM approach to modeling local structure and properties of molecules in the solid state. Judged from the selected examples, the approach can be very successful and can be systematically improved by increasing the QM region. There may well be cases where the approach will not perform so well: most likely highly polarizable systems where the point charge approximation of the environment leads to over-polarization of the QM region density, or where considerable charge transfer between molecules takes place. Also, the accuracy or transferability of the vdW parameters that define the 6-12 Lennard-Jones potentials deserves further scrutiny.

In principle, both of these problems can be alleviated by increasing the QM region, but in practice this can become very expensive even for small molecules if many nearest neighboring molecules need to be included and may actually become more expensive than a periodic DFT calculation. By using small basis sets (possibly with effective core potentials), this can often be made computationally tractable. Point charge smearing around the QM region or frozen-density embedding might be a way to improve upon our model.

We have focused on geometry optimizations in the solid state which are crucial for subsequent molecular property calculations and took examples from the blossoming field of solid-state NMR spectroscopy. We note that this protocol should also be suitable for other molecular property calculations, such as EPR, Mössbauer, IR, and Raman frequencies; absorption spectra; etc. The calculations could also be adapted to study long-range effects of static disorder on these properties, at no extra cost if that disorder is effected in the MM cluster. In contrast, modeling disorder under periodic boundary conditions can become prohibitively expensive if very large supercells are needed.

For many small molecular crystals, the cost of a periodic DFT optimization may be more favorable than the QM/MM approach we take for local geometry optimization. In such cases, the periodic DFT structure may simply be used as input in our QM/MM protocol with the optimization steps of the protocol (loop B etc.) skipped and only single-point QM/MM performed in order to calculate self-consistent point charges for subsequent molecular property calculations. We expect QM/MM geometry optimizations to be useful, however, when rather large unit cells are encountered, making periodic DFT optimizations prohibitively expensive or when very accurate geometries are required, making the use of localized basis sets and/or higher accuracy electronic structure methods an attractive feature of our QM/MM approach.

Finally, we note that the starting crystal structure information is a crucial aspect of our method. These calculations will thus be mainly useful for detailed analysis of molecules in crystals, or for refinement of structural data of lower quality, and will hardly lead to real predictions of solids in the absence of any structure information. However, as the method does not necessarily need very accurate structural data, this information may in the future come from crystal structure prediction algorithms that are beginning to become more and more successful in recent years.[97] Assessment of three-dimensional molecular structures from X-ray powder diffraction may also become attractive, as the limits of this technique in terms of molecular size and complexity are being expanded steadily.

■ ASSOCIATED CONTENT

Supporting Information. QM/MM-NPA optimized geometries of the larger QM regions of molecules **1**-**4** as well as periodic DFT optimized geometries of **3** and **4** in Cartesian coordinates. This material is available free of charge via the Internet at http://pubs.acs.org.

■ AUTHOR INFORMATION

Corresponding Author

*E-mail: buehl@st-andrews.ac.uk.

Notes

The authors declare no competing financial interest.

■ ACKNOWLEDGMENT

This work was supported by EaStChem via the EaStChem Research Computing facility and a local Opteron PC cluster maintained by H. Früchtl. We thank Tom Keal and Paul Sherwood for help with the Chemshell program.

■ REFERENCES

(1) Sorouri, A.; Foulkes, W. M. C.; Hine, N. D. M. *J. Chem. Phys.* **2006**, *124*, 064105. Paier, J.; Diaconu, C. V.; Scuseria, G. E.; Guidon, M.; VandeVondele, J.; Hutter, J. *Phys. Rev. B* **2009**, *80*, 174114.

(2) See, e.g., the discussion in: Senn, H. M.; Thiel, W. *Top. Curr. Chem.* **2007**, *268*, 173–290.

(3) Hu, L.; Söderhjelm, P.; Ryde, U. *J. Chem. Theory Comput.* **2011**, *7*, 761–777.

(4) Senn, H. M.; Thiel, W. *Angew. Chem., Int. Ed.* **2009**, *48*, 1198–1229.

(5) Gao, J. *Acc. Chem. Res.* **1996**, *29*, 298–305.

(6) Acevedo, O.; Jorgensen, W. L. *Acc. Chem. Res.* **2009**, *43*, 142–151.

(7) Moore, E. A. *Chem. Modell.* **2008**, *5*, 119–149.

(8) Catlow, R.; Bell, R.; Cora, F.; French, S. A.; Slater, B.; Sokol, A. *Annu. Rep. Prog. Chem. Sect. A: Inorg. Chem.* **2005**, *101*, 513–547.

(9) Sherwood, P.; de Vries, A. H.; Guest, M. F.; Schreckenbach, G.; Catlow, C. R. A.; French, S. A.; Sokol, A. A.; Bromley, S. T.; Thiel, W.; Turner, A. J.; Billeter, S.; Terstegen, F.; Thiel, S.; Kendrick, J.; Rogers, S. C.; Casci, J.; Watson, M.; King, F.; Karlsen, E.; Sjøvoll, M.; Fahmi, A.; Schäfer, A.; Lennartz, C. *THEOCHEM* **2003**, *632*, 1.

(10) Catlow, C. R. A.; French, S. A.; Sokol, A. A.; Thomas, J. M. *Phil. Trans. R. Soc. London, Ser. A* **2005**, *363*, 913–935.

(11) Sokol, A. A.; Bromley, S. T.; French, S. A.; Catlow, C. R. A.; Sherwood, P. *Int. J. Quantum Chem.* **2004**, *99*, 695.

(12) For selected implementations and reviews of periodic NMR calculations, see e.g.: (a) Pickard, C. J.; Mauri, F. *Phys. Rev. B* **2011**, *69*, 245101. (b) Harris, R. K.; Hodgkinson, P.; Pickard, C. J.; Yates, J. R.; Zorin, V *Magn. Reson. Chem.* **2007**, *45*, S174–S186. (c) Sebastiani, D.; Parrinello, M. *J. Phys. Chem. A* **2001**, *105*, 1951–1958. (d) Skachkov, D.; Krykunov, M.; Kadantsev, E.; Ziegler, T *J. Chem. Theory Comput.* **2010**, *6*, 1650–1659. (e) Skachkov, D.; Krykunov, M.; Ziegler, T *Can. J. Chem.* **2011**, *89*, 1150–1161.

(13) Bühl, M.; Wrackmeyer, B. *Magn. Reson. Chem.* **2010**, *48*, S61–S68.

(14) Bochevarov, A. D.; Friesner, R. A.; Lippard, S. J. *J. Chem. Theory Comput.* **2010**, *6*, 3735–3749.
(15) Sandala, G. M.; Hopmann, K. H.; Ghosh, A.; Noodleman, L. *J. Chem. Theory Comput.* **2011**, *7*, 3232–3247.
(16) Chatterjee, P. B.; Goncharov-Zapata, O.; Quinn, L. L.; Hou, G.; Hamaed, H.; Schurko, R. W.; Polenova, T.; Crans, D. C. *Inorg. Chem.* **2011**, *50*, 9794–9803.
(17) Cuny, J.; Sykina, K.; Fontaine, B.; Le Polles, L.; Pickard, C. J.; Gautier, R. *Phys. Chem. Chem. Phys.* **2011**, *13*, 19471–19479.
(18) Stueber, D. *Concepts Magn. Reson. Part A* **2006**, *28A*, 347–368.
(19) Weber, J.; Schmedt auf der Günne, J. *Phys. Chem. Chem. Phys.* **2010**, *12*, 583–603.
(20) Stueber, D.; Guenneau, F. N; Grant, D. M. *J. Chem. Phys.* **2001**, *114*, 9236. Stueber, D.; Grant, D. M. *J. Am. Chem. Soc.* **2002**, *124*, 10539–10551. Stueber, D.; Orendt, A. M.; Facelli, J. C.; Parry, R. W.; Grant, D. M. *Solid State Nucl. Magn. Reson.* **2002**, *22*, 29–49. Stueber, D.; Grant, D. M. *Solid State Nucl. Magn. Reson.* **2002**, *22*, 439–457. Orendt, A. M. *Magn. Reson. Chem.* **2006**, *44*, 385–389.
(21) Bjornsson, R.; Früchtl, H.; Bühl, M. *Phys. Chem. Chem. Phys.* **2011**, *13*, 619–627.
(22) Götz, K.; Meier, F.; Gatti, C.; Burow, A. B.; Sierka, M.; Sauer, J.; Kaupp, M. *J. Comput. Chem.* **2010**, *31*, 2568–2576.
(23) Ferenczy, G. G.; Csonka, G. I.; Náray-Szabó, G.; Ángyán, J. G. *J. Comput. Chem.* **1998**, *19*, 38–50.
(24) Swerts, B.; Van Droogenbroeck, J.; Peeters, A.; Van Alsenoy, C. *J. Phys. Chem. A* **2002**, *106*, 4245–4250.
(25) Wen, S.; Beran, G. J. O. *J. Chem. Theory Comput.* **2011**, *7*, 3733–3742.
(26) Kimmel, A. V.; Ramo, D. M.; Sushko, P .V.; Shluger, A. L.; Kuklja, M. M. *Phys. Rev. B* **2009**, *80*, 134108.
(27) Kaminski, R.; Schmokel, M. S.; Coppens, P. *J. Phys. Chem. Lett.* **2010**, *1*, 2349–2353.
(28) Torras, J.; Bromley, S.; Bertran, O.; Illas, F. *Chem. Phys. Lett.* **2008**, *457*, 154–158.
(29) See, e.g.: Facelli *Prog. NMR Spectrosc.* **2011**, *58*, 176–201.
(30) See, e.g.: Bühl, M.; van Mourik, T. *Wiley Interdisciplinary Reviews: Computational Molecular Science* **2011**, *1*, 634–647.
(31) Schmidt, J.; Hoffmann, A.; Spiess, H. W.; Sebastiani, D. *J. Phys. Chem. B* **2006**, *110*, 23204–23210.
(32) Yates, J. R.; Dobbins, S. E.; Pickard., C. J.; Mauri, F.; Ghi, P. Y.; Harris, R. K. *Phys. Chem. Chem. Phys.* **2005**, *7*, 1402–1407.
(33) Johnston, J. C.; Iuliucci, R. J.; Facelli, J. C.; Fitzgerald, G.; Mueller, K. T. *J. Chem. Phys.* **2009**, *131*, 144503.
(34) Cuny, J.; Messaoudi, S.; Alonzo, V.; Furet, E.; Halet, J. F.; Le Fur, E.; Ashbrook, S. E.; Pickard, C. J.; Gautier, R.; Le Polles, L. *J. Comput. Chem.* **2008**, *29*, 2279–2287.
(35) Rappe, A. K.; Casewit, C. J.; Colwell, K. S.; Goddard, W. A., III; Skiff, W. M. *J. Am. Chem. Soc.* **1992**, *114*, 10024–10035.
(36) Bayly, C. I.; Cieplak, P.; Cornell, W. D.; Kollman, P. A. *J. Chem. Phys.* **1993**, *97*, 10269–10280.
(37) Reed, A.; Weinstock, R. B.; Weinhold, F. *J. Chem. Phys.* **1985**, *83*, 735–746.
(38) Mulliken, R. S. *J. Chem. Phys.* **1955**, *23*, 1833–1840.
(39) ChemShell, a Computational Chemistry Shell. See www.chemshell.org (accessed Oct 31, 2011).
(40) Sing, U. C.; Kollman, P. A. *J. Comput. Chem.* **1984**, *5*, 129. Besler, B. H.; Merz, K. M.; Kollman, P. A. *J. Comput. Chem.* **1990**, *11*, 431.
(41) Senthilkumar, K.; Mujika, J. I.; Ranaghan, K. E.; Manby, F. R.; Mulholland, A. J.; Harvey, J. N. *J. R. Soc. Interface* **2008**, *5*, S207–S216.
(42) Gordon, M. S.; Slipchenko, L.; Li, H.; Jensen, J. H. *Ann. Rep. Comp. Chem.* **2007**, *3*, 177–193. Gordon, M. S.; Fedorov, D. G.; Pruitt, S. R.; Slipchenko, L. V. *Chem. Rev.* **2011**, DOI: 10.1021/cr200093j.
(43) Wesolowski, T. A.; Warshel, A. *J. Phys. Chem.* **1993**, *97*, 8050.Wesolowski, T. A. In *Computational Chemistry: Reviews of Current Trends - Vol. 10*; World Scientific, 2006. Jacob, C. R.; Neugebauer, J.; Visscher, L. *J. Comput. Chem.* **2007**, *6*, 1011–1018. Jacob, C. R.; Neugebauer, J.; Jensen, L.; Visscher, L. *Phys. Chem. Chem. Phys.* **2006**, *8*, 2349–2359.
(44) Eichinger, M.; Tavan, P.; Hutter, J.; Parrinello, M. *J. Chem. Phys.* **1999**, *110*, 10452–10467. Das, D.; Eurenius, K. P.; Billings, E.; Sherwood P.; Chatfield, D. C.; Hodoscek, M.; Brooks, B. R. *J. Chem. Phys.* **2002**, *117*, 10534. Amara, P.; Field, M. J. *Theor. Chem. Acc.* **2003**, *109*, 43–52. Wang, B.; Truhlar, D. G. *J. Chem. Theory Comput.* **2010**, *6*, 3330–3342. Wang, B.; Truhlar, D. G. *Phys. Chem. Chem. Phys.* **2011**, *13*, 10556–10564.
(45) *CPMD*, version 3.13.1; IBM Corp.: Endicott, NY, 1990; MPI für Festkörperforschung Stuttgart: Stuttgart, Germany, 1997.
(46) Troyanov, S. I. *Russ. J. Inorg. Chem.* **2005**, *50*, 1727.
(47) Compared to the previous BP86-D structure in ref 21, which used an 80 Ry cutoff, the VO and VCl distances changed by −0.00574 Å and +0.0027 Å, respectively.
(48) A further increase in the cutoff, as well as *k*-point sampling using a 4 × 2 × 2 Monkhorst−Pack grid, resulted in only minor changes of geometrical parameters and NMR parameters in subsequent property calculations.
(49) Smith, W.; Yong, C.; Rodger, P. *Mol. Simul.* **2002**, *28*, 385.
(50) *Turbomole*, version 6.0.5; Turbomole GmbH: Karlsruhe, Germany, 2008. See: www.turbomole.com (accessed Oct 31, 2011).
(51) Frisch, M. J.; Trucks, G. W.; Schlegel, H. B.; Scuseria, G. E.; Robb, M. A.; Cheeseman, J. R.; Scalmani, G.; Barone, V.; Mennucci, B.; Petersson, G. A.; Nakatsuji, H.; Caricato, M.; Li, X.; Hratchian, H. R.; Izmaylov, A. F.; Bloino, J.; Zheng, G.; Sonnenberg, J. L.; Hada, M.; Ehara, M.; Toyota, K.; Fukuda, R.; Hasegawa, J.; Ishida, M.; Nakajima, T.; Honda, Y.; Kitao, O.; Nakai, H.; Vreven, T.; Montgomery, J. R., Jr.; Peralta, J. A.; Ogliaro, F.; Bearpark, M.; Heyd, J. J.; Brothers, E.; Kudin, K. N.; Staroverov, V. N.; Kobayashi, R.; Normand, J.; Raghavachari, K.; Rendell, A.; Burant, J. C.; Iyengar, S. S.; Tomasi, J.; Cossi, M.; Rega, N.; Millam, J. M.; Klene, M.; Knox, J. E.; Cross, J. B.; Bakken, V.; Adamo, C., Jaramillo, J.; Gomperts, R.; Stratmann, R. E.; Yazyev, O.; Austin, A. J.; Cammi, R.; Pomelli, C.; Ochterski, J. W.; Martin, R. L.; Morokuma, K.; Zakrzewski, V. G.; Voth, G. A.; Salvador, P.; Dannenberg, J. J.; Dapprich, S.; Daniels, A. D.; Farkas, O.; Foresman, J. B.; Ortiz, J. V.; Cioslowski, J.; Fox, D. J. *Gaussian 09*, Revision B.01.; Gaussian Inc.: Wallingford, CT, 2009.
(52) Valiev, M.; Bylaska, E.; Wang, D.; Kowalski, K.; Govind, N.; Straatsma, T.; van Dam, H.; Nieplocha, J.; Apra, E.; Windus, T.; de Jong, W. *Comput. Phys. Commun.* **2010**, *181*, 1477–1489.
(53) Neese, F. *ORCA*; University of Bonn: Bonn, Germany, 2010. http://www.thch.uni-bonn.de/tc/orca (accessed Oct 31, 2011).
(54) GAMESS-UK is a package of ab initio programs. http://www.cfs.dl.ac.uk/gamess-uk/index.shtml (accessed Oct 31, 2011).
(55) Guest, M. F.; Bush, I. J.; van Dam, H. J. J.; Sherwood, P.; Thomas, J. M. H.; van Lenthe, J. H.; Havenith, R. W. A; Kendrick *J. Mol. Phys.* **2005**, *103*, 719.
(56) Werner, H.-J.; Knowles, P. J.; Lindh, R.; Manby, F. R.; Schütz, M.; Celani, P.; Korona, T.; Rauhut, G.; Amos, R. D.; Bernhardsson, A.; Berning, A.; Cooper, D. L.; Deegan, M. J. O.; Dobbyn, A. J.; Eckert, F.; Hampel, C.; Hetzer, G.; Lloyd, A. W.; McNicholas, S. J.; Meyer, W.; Mura, M. A.; Nicklass, A.; Palmieri, P.; Pitzer, R.; Schumann, U.; Stoll, H.; Stone, A. J.; Tarroni, R.; Thorsteinsson, T. *MOLPRO*; University College Cardiff Consultants Limited: Cardiff, U.K., 2010.
(57) Thiel, W. *MNDO99*; Max-Planck-Institut für Kohlenforschung: Mülheim an der Ruhr, Germany, 2004.
(58) Kästner, J.; Carr, J. M.; Keal, T. W.; Thiel, W.; Wander, A.; Sherwood, P. *J. Phys. Chem. A* **2009**, *113*, 11856.
(59) Reeve, S. W.; Burns, W. A.; Lovas, F. J.; Suenram, R. D.; Leopold, K. R. *J. Phys. Chem.* **1993**, *97*, 10630–10637.
(60) Burns, W. A.; Leopold, K. R. *J. Am. Chem. Soc.* **1993**, *115*, 11622–11623.
(61) Bühl, M.; Steinke, T.; Schleyer, P. v. R.; Boese, R. *Angew. Chem., Int. Ed. Engl.* **1991**, *30*, 1160. Cremer, D.; Olsson, L.; Reichel, F.; Kraka, E. *Isr. J. Chem.* **1993**, *33*, 369. Klooster, W. T.; Koetzle, T. F.; Siegbahn, P. E. M.; Richardson, T. B.; Crabtree, R. H. *J. Am. Chem. Soc.* **1999**, *121*, 6337–6343. Hofmann, M.; Schleyer, P. v. R. *J. Am. Chem. Soc.* **1994**, *116*, 4947.

(62) Jiao, H.; Schleyer, P. v. R. *J. Am. Chem. Soc.* **1994**, *116*, 7429–7430.
(63) Iglesias, E.; Sordo, T. L.; Sordo, J. A. *Chem. Phys. Lett.* **1995**, *248*, 179–181. Cabaleiro-Lago, E. M.; Rios, M. A. *Chem. Phys. Lett.* **1998**, *294*, 272–276. Venter, G.; Dillen, J. *J. Phys. Chem. A* **2004**, *108*, 8378–8384.
(64) Phillips, J. A.; Cramer, C. J. *J. Chem. Theory Comput.* **2005**, *1*, 827–833.
(65) Janesko, B. G. *J. Chem. Theory Comput.* **2010**, *6*, 1825–1833.
(66) Becke, A .D. *J. Chem. Phys.* **1993**, *98*, 5648–5652.
(67) Lee, C. T.; Yang, W. T.; Parr, R. G. *Phys. Rev. B* **1988**, *37*, 785–789.
(68) Perdew, J. P. In *Electronic Strucure of Solids*; Ziesche, P., Eischrig, H., Eds.; Akademie Verlag: Berlin, 1991. (b) Perdew, J. P.; Wang, Y. *Phys. Rev. B* **1992**, *45*, 13244–13249.
(69) Grimme, S. *J. Chem. Phys.* **2006**, *124*, 034108. Goerigk, L.; Grimme, S. *J. Chem. Theory Comput.* **2011**, *7*, 291–309.Kozuch, S.; Martin, J. M. L. *Phys. Chem. Chem. Phys.* DOI: 10.1039/C1CP22592H
(70) Dunning, T. H., Jr. *J. Chem. Phys.* **1989**, *90*, 1007. Kendall, R. A.; Dunning, T. H.; Harrison, R. J. *J. Chem. Phys.* **1992**, *96*, 6796.
(71) Hehre, W. J.; Ditchfield, R.; Pople, J. A. *J. Chem. Phys.* **1972**, *56*, 2257. Hariharan, P. C.; Pople, J. A. *Theor. Chim. Acta.* **1973**, *28*, 213.
(72) Wiberg, K. B.; Rablen, P. R. *J. Comput. Chem.* **1993**, *14*, 1504–1518.
(73) Calhorda, M. J.; Pregosin, P. S.; Veiros, L. F. *J. Chem. Theory Comput.* **2007**, *3*, 665.
(74) Fernandez, I.; Hermatschweiler, R.; Breher, F.; Pregosin, P. S.; Veiros, L. F.; Calhorda, M. J. *Angew. Chem., Int. Ed.* **2006**, *45*, 6386.
(75) Waller, M. P.; Braun, H.; Hojdis, N.; Bühl, M. *J. Chem. Theory Comput.* **2007**, *3*, 2234–2242. Bühl, M.; Reimann, C.; Pantazis, D. A.; Bredow, T.; Neese, F. *J. Chem. Theory Comput.* **2008**, *4*, 1449–1459.
(76) Perdew, J. P.; Burke, K.; Ernzerhof, M. *Phys. Rev. Lett.* **1996**, *77*, 3865. Perdew, J. P.; Burke, K.; Ernzerhof, M. *Phys. Rev. Lett.* **1997**, *78*, 1396. Adamo, C.; Barone, V. *J. Chem. Phys.* **1999**, *110*, 6158.
(77) Truhlar, D. G.; Kulkarni, A. D. *J. Chem. Theory Comput.* **2011**, *7*, 2325–2332.
(78) Zhao, Y.; Truhlar, D. G. *J. Chem. Phys.* **2006**, *125*, 194101.
(79) Zhao, Y.; Truhlar, D. *Theor. Chem. Acc.* **2008**, *120*, 215.
(80) Zhao, Y.; Truhlar, D. G. *J. Chem. Phys.* **2008**, *128*, 184109.
(81) Chai, J.-D.; Head-Gordon, M. *Phys. Chem. Chem. Phys.* **2008**, *10*, 6615.
(82) Jacobsen, H. *J. Chem. Theory Comput.* **2011**, *7*, 3019–3025.
(83) Weigend, F.; Ahlrichs, R. *Phys. Chem. Chem. Phys.* **2005**, *7*, 3297.
(84) Grimme, S. *J. Comput. Chem.* **2006**, *27*, 1787.
(85) This seems reasonable, as equilibrium geometries are compared to thermally averaged structures. Inclusion of zero-point corrections and thermal motion tends to increase metal−ligand equilibrium distances by a few to several picometers, see e.g.: Waller, M. P.; Braun, H.; Hojdis, N.; Bühl, M. *J. Chem. Theor. Comput.* **2007**, *3*, 2234–2242.
(86) Moellmann, J.; Grimme, S. *Phys. Chem. Chem. Phys.* **2010**, *12*, 8500–8504.
(87) Becke, A. D. *Phys. Rev. A* **1988**, *38*, 3098–100.
(88) Perdew, J. P. *Phys. Rev. B* **1986**, *33*, 8822. Perdew, J. P. *Phys. Rev. B* **1986**, *34*, 7406.
(89) The EFG determines the nuclear quadrupole coupling (NQC) tensor, given in the form of an isotropic NQC constant, $C_Q = (e^2QV_{zz})/h$, and its asymmetry parameter, $\eta_Q=(V_{yy} - V_{xx})/V_{zz}$, where V_{zz}, V_{yy}, and V_{xx} are the principal components of the EFG tensor ($|V_{zz}| \geq |V_{xx}| \geq |V_{yy}|$). The chemical-shift tensor is reported in the form of the isotropic shift δ, its anisotropy $\delta_\sigma = \delta_{zz} - \delta_{iso}$, and its asymmetry parameter $\eta_\sigma = (\delta_{yy} - \delta_{xx})/\delta_{zz}$ where $|\delta_{zz} - \delta_{iso}| \geq |\delta_{xx} - \delta_{iso}| \geq |\delta_{yy} - \delta_{iso}|$ according to the Haeberlen−Mehring−Spiess convention.
(90) Galy, J.; Enjalbert, R.; Jugie, G.; Strähle, J. *J. Solid State Chem.* **1983**, *47*, 143.
(91) Cornman, C. R.; Colpas, G. J.; Hoeschele, J. D.; Kampf, J.; Pecoraro, V. L. *J. Am. Chem. Soc.* **1992**, *114*, 9925.
(92) Bjornsson, R.; Bühl, M. *Dalton Trans.* **2010**, *39*, 5319–5324.
(93) Bjornsson, R.; Bühl, M. Manuscript in preparation.
(94) Geethalakshmi, K. R.; Waller, M. P.; Bühl, M. *Inorg. Chem.* **2007**, *46*, 11297–11307.
(95) Rehder, D.; Polenova, T.; Bühl, M. *Annu. Rep. NMR Spectrosc.* **2007**, *62*, 49–114.
(96) Sebastiani, D.; Rothlisberger, U. *J. Phys. Chem. B.* **2004**, *108*, 2807–2815.
(97) Neumann, M. A.; Leusen, F. J. J.; Kendrick, J. *Angew. Chem., Int. Ed.* **2008**, *47*, 2427–2430. Chan, H. C.; Kendrick, J.; Leusen, F. J. J. *Angew. Chem., Int. Ed.* **2011**, *50*, 2979–2981. Woodley, S. M.; Catlow, R. *Nat. Mater.* **2008**, *7*, 937–946. Lehmann, C. W. *Angew. Chem., Int. Ed.* **2011**, *50*, 5616–5617. Bardwell, D. A. *Acta Crystallogr.* **2011**, *B67*, 535–551.